The behavior and modelling of the vibrational-to-translational temperature ratio at long time scales in CO_2 vibrational kinetics

Moreno, Sergio H.; Stankiewicz, Andrzej I.; Stefanidis, Georgios D.

DOI
10.1039/c9re00255c

Publication date
2019

Document Version
Accepted author manuscript

Published in
Reaction Chemistry and Engineering

Behavior and modelling of the vibrational-to-translational temperature ratio at long time scales in CO_2 vibrational kinetics.

Sergio H. Moreno [a], *Andrzej I. Stankiewicz* [a], *Georgios D. Stefanidis* [b,*]

[a] *Intensified Reaction & Separation Systems, Process & Energy Laboratory, Delft University of Technology, Leeghwaterstraat 39, 2628 CB, Delft, The Netherlands*

[b] *Chemical Engineering Department, Katholieke Universiteit Leuven, Celestijnenlaan 200f, 3001 Leuven (Heverlee), Belgium*

[*] *Corresponding author: Georgios D. Stefanidis, e-mail:* georgios.stefanidis@kuleuven.be

Abstract

Non-thermal microwave plasma reactors can efficiently split the CO_2 molecule. However, big challenges remain before this technology becomes a feasible industrial technology. Computer modelling can be very useful to tackle such challenges. Detailed kinetic modelling is commonly used to get insights into the complex vibrational kinetics of CO_2 as vibrational excitation is strongly related to the energy efficiency in the dissociation process. The vibrational-to-translational temperature ratio has been identified as a key variable to achieve high energy efficiencies. This ratio has also been used to simplify detailed CO_2 vibrational kinetics, notably reducing the number of species and reactions required to model the non-thermal plasma. In this paper we use an isothermal reaction kinetics model to study the vibrational kinetics of CO_2 under the typical conditions used in non-thermal microwave plasma experiments. The importance of the different collisional processes is evaluated throughout the conditions and timescales at which CO_2 dissociation takes place. The long timescale behavior of the vibrational-to-translational temperature ratio at different conditions is discussed in detail. It is shown that its behavior at increasing gas temperatures can be fitted to an expression that incorporates the Landau-Teller temperature dependence. This is confirmed by average Adjusted R-square values higher than 0.99 and average Root Mean Square Error values smaller than 0.22 at low gas temperatures. The limitations of the fitting expression are also discussed, specially the conditions and timescales at which it yields better results.

Keywords

CO_2 dissociation, CO_2 plasma, microwave plasma, vibrational kinetics

1. Introduction

Non-thermal microwave plasma reactors have been experimentally proven to be successful in splitting the CO_2 molecule [1–9]. Moreover, the vibrational excitation of the asymmetric stretching mode has been identified as the means to achieve energy efficiencies as high as 90% [10]. It is claimed that the energy stored in this vibrational mode can effectively reduce the energy barrier of endothermic reactions. In such way, the dissociation reaction is carried out efficiently, breaking the CO_2 molecule with less heating of the gas. In this dissociation mechanism, low-lying asymmetric vibrational states get excited through electron collisions and they transfer their energy to higher vibrational states thus creating an overpopulation of highly energetic states that can easily dissociate. Further information on this mechanism can be found elsewhere [10,11].

Some pieces are still missing in the puzzle of making CO_2 dissociation in microwave plasma reactors a feasible industrial technology, e.g. the well-known trade-off between high chemical conversion and high energy efficiency. In this regard, computer modelling is a resourceful tool to cope with the challenges ahead. Diverse aspects hindering plasma reactors technology can be tackled through computer modelling, for instance, the fundamental understanding of molecular processes can be improved, the reaction rates constants can be validated and the scalability of the reactors can be explored.

Different modelling approaches have been used to get insights into the plasma processes and the reactor performance [12–22]. The detailed study of vibrational kinetics requires the calculation of population densities for different vibrational energy levels, usually the full span, from ground state to dissociation limit. The complete vibrational distribution of a vibrational mode is determined by including all its vibrational levels in the study and analyzing their different interactions. In such cases, two approaches are usually employed. The most common approach is the State-To-State (STS) kinetic model, in which energy states of atoms and molecules are considered as separate species and their relevant interactions are considered as independent reactions (elementary steps). In this approach the energy levels are considered discrete and a large number of species and reactions are not rare. A more recent approach [15,16] replaces the discrete energy levels by a continuous vibrational energy function. The equation for the rate of change of the species is thus replaced by a drift-diffusion Fokker-Plank equation, with transport parameters computed from rate constants of state to state

interactions. This approach has the potential to be much more computationally efficient than the traditional STS kinetic model approach.

Additional efforts have been addressed to reduce the very complex STS kinetics models into manageable kinetics models suitable to multidimensional models, which are intended to improve the design and performance of plasma reactors [23,24]. In our previous research on the matter we proposed a reduction methodology that employs the vibrational to translation temperature ratio as a key parameter for the reduction of the vibrational kinetics [23]. In this reduction methodology, all asymmetric vibrational levels of CO_2 are grouped within the fictitious species CO_2* and the vibrational to translation temperature ratio is used to compute weighted algebraic rate constants of reactions involving CO_2*. The application of this methodology results in a considerable reduction of the number of reactions and species required to describe the vibrationally enhanced dissociation of CO_2. Recently, the reduction methodology has been used in a two-step modelling approach to model a surface wave microwave plasma reactor [25]. The importance of this temperature ratio has also been discussed in other works [15,16,26], where it is mentioned that the non-equilibrium effect leading to the vibrationally enhanced dissociation of CO_2 is better exploited at high values of this ratio. Higher values of the temperature ratio lower the energy level for the point of no return, beyond which vibrationally excited molecules most likely increase their vibrational energy and dissociate.

In this paper we use an isothermal STS reaction kinetics model to study the vibrational kinetics of CO_2, particularly the kinetics of the asymmetric vibrational mode. In addition, the effect of symmetric sublevels on the kinetics of asymmetric levels is also investigated. The analysis is limited to the typical experimental conditions used for pure CO_2 dissociation in non-thermal microwave plasma and the timescales at which this dissociation takes place. The relevance of the different collisional processes is also evaluated throughout the conditions and timescales. Finally, the long timescale behavior of the vibrational to translational temperature ratio is discussed in detailed as it has been identified as a key parameter to achieve an efficient dissociation.

2. Model description

The reaction kinetics model solves the particle conservation equation for all the species in the plasma. It represents the plasma as point in space, disregarding dimensionality and transport.

The rate of change of a species is given by the chemical reactions and is computed from the following equation

$$\frac{dn_i}{dt} = \sum_k \left(\nu_{i,k}^{\mathrm{R}} - \nu_{i,k}^{\mathrm{L}}\right)\left(k_{k,\mathrm{f}} \prod_i n_i^{\nu_{i,k}^{\mathrm{L}}} - k_{k,\mathrm{r}} \prod_i n_i^{\nu_{i,k}^{\mathrm{R}}}\right) \tag{1}$$

Where n_i is the number density of the species i, $\nu_{i,k}^{\mathrm{R(L)}}$ is the right(left)-hand-side stoichiometric coefficient of the species i in reaction k and $k_{k,\mathrm{f(r)}}$ is the forward (reverse) reaction rate constant for reaction k. Elementary reactions between specific energy states of the CO_2 molecule are included in this STS reaction kinetics model. The electron density n_e and electron temperature T_e are assumed constant, as well as the heavy species temperature T.

Table 1. Species considered in the CO_2 model.

Type	Species
Neutral ground state (1)	CO_2
Vibrationally excited states (84)	$CO_2\nu_a$, $CO_2\nu_b$, $CO_2\nu_c$, $CO_2\nu_n$, $CO_2\nu_{n,a}$, $CO_2\nu_{n,b}$, $CO_2\nu_{n,c}$
Charged species (2)	CO_2^+, e

The species considered in the model are CO_2 species and electrons, see Table 1. To preserve the electroneutrality of the plasma the CO_2 ion density is made equal to the electron density. The analysis of the CO_2 vibrational kinetics is the objective of this paper and therefore no other species different than CO_2 are included. Moreover, no specific rotationally or electronically excited states of CO_2 are considered, as they have no direct influence in the vibrational kinetics. These excited states affect the vibrational kinetics through the variation of the electron temperature, which is a parameter of this kinetic model. The vibrational state of the CO_2 molecule is specified by three quantum numbers $(i_1\ i_2\ i_3)$, indicating the vibrational levels in the symmetric stretching, symmetric bending and asymmetric stretching vibrational modes, respectively. Symmetric bending levels have a degeneracy of $i_2 + 1$ as the bending can take place in orthogonal planes. Stretching modes are non-degenerate. Furthermore, the vibrational levels $((i_1 + 1)\ i_2\ i_3)$ and $(i_1\ (i_2 + 2)\ i_3)$ are coupled due to the proximity of their energy, they coexist and are therefore grouped into a single species. In this case, the total degeneracy of the species is the sum of the degeneracies of the grouped states and is referred to as statistical weight.

Table 2. Vibrationally excited species, their energies and statistical weights.

Species	**Vibrational states** $(i_1\ i_2\ i_3)$	**Energy (eV)** $E_{(i_1\ i_2\ i_3)}$	**Statistical Weight** $\sum(i_2+1)$
$CO_2\nu_a$	(0 1 0)	0.083	2
$CO_2\nu_b$	(0 2 0) + (1 0 0)	0.166	4
$CO_2\nu_c$	(0 3 0) + (1 1 0)	0.250	6
$CO_2\nu_n$	(0 0 *n*)	$E_{(0\ 0\ n)}$	1
$CO_2\nu_{n,a}$	(0 1 *n*)	$E_{(0\ 1\ n)}$	2
$CO_2\nu_{n,b}$	(0 2 *n*) + (1 0 *n*)	$E_{(0\ 2\ n)}$	4
$CO_2\nu_{n,c}$	(0 3 *n*) + (1 1 *n*)	$E_{(0\ 3\ n)}$	6

The first three symmetric bending levels are included in the model as purely symmetric vibrational species and as "sublevels" of asymmetric vibrational states, see Table 2. The symmetric levels are denoted by the subscripts *a*, *b* and *c*, and the asymmetric vibrational levels are denoted by the index *n*. The vibrational energy levels can be computed from the triatomic anharmonic oscillator model, which to the second order of approximation reads [27]

$$\frac{E_{(i_1\ i_2\ i_3)}}{hc} = \sum_n \omega_n(i_n + d_n/2) + \sum_{m\geq n} x_{nm}(i_n + d_n/2)\,(i_m + d_m/2) + x_{l_2 l_2} l_2^2 \qquad (2)$$

Where $E_{(i_1\ i_2\ i_3)}$ is the vibrational energy, h is the Planck constant, c the speed of light, i_n and d_n the vibrational quantum number and the degeneracy of the vibrational mode *n*, respectively. The special quantum number l_2 related to the quasi-rotation around the principal axis of the molecule is assumed to be 0. The spectroscopic constants are given in Table 3.

Table 3. Spectroscopic constants for computing the vibrational energy levels of CO_2 [27].

Constant	**Value (1/cm)**
ω_1	1354.31
ω_2	672.85
ω_3	2396.32
x_{11}	-2.93
x_{12}	-4.61
x_{13}	-19.82
x_{22}	1.35
x_{23}	-12.31
x_{33}	-12.47
$x_{l_2 l_2}$	-0.97

According to this model and these spectroscopic constants, the first asymmetric level has an energy of 0.29 eV and the asymmetric level 21, with an energy of 5.47 eV, lies in the dissociation limit of the molecule (5.5 eV). It is assumed that this level is the highest asymmetric level before the molecule dissociates. Thus, the index n in $CO_2\nu_n$ runs from 1 to 21, whereas in $CO_2\nu_{n,(a,b,c)}$ runs from 1 to 20. Figure 1 shows the vibrational energy scale with selected species in the model. It is clear from this Figure that the symmetric levels are closer together and that $CO_2\nu_{n-1,(a,b,c)} < CO_2\nu_n$, therefore the "sublevel" designation. Moreover, due to the anharmonicity of the molecule, the vibrational levels come closer as the energy increases.

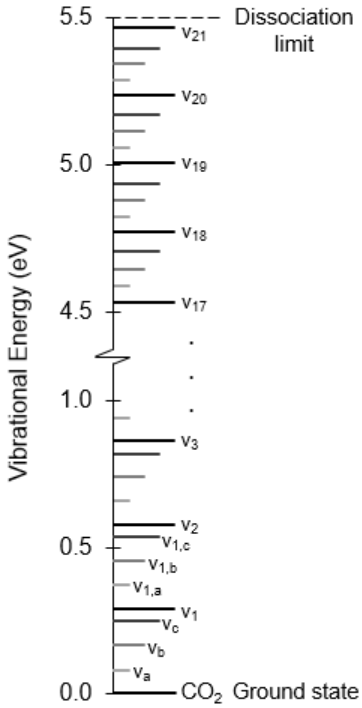

Fig. 1. Vibrational energy levels of selected CO_2 species in the model, from equation 2. Asymmetric level 21 is the highest asymmetric level, thus, for $CO_2\nu_n$ $n = 1, 2, \ldots, 21$, whereas for $CO_2\nu_{n,(a,b,c)}$ $n = 1, 2, \ldots, 20$. See also Supporting Information.

The set of reactions is based on the vibrational kinetics developed by Kozak et al [12,13]. Notable differences are the addition of symmetric sublevels and their reactions, the gradual relaxation of symmetric (sub)levels *b* and *c*, and the assumption of a Maxwellian Electron Energy Distribution Function (EEDF). Dissociation reactions are excluded as well as reactions between charged species. The considered reactions are thus limited to electron impact vibrational excitation and vibrational relaxation, along with their reverse reactions. The rate constants for the latter are computed from the detailed balance principle, which

ensures that under thermal equilibrium conditions at a temperature T^* the correct densities for the vibrational levels are obtained

$$k_{k,r} = k_{k,\mathrm{f}} \frac{\prod g^L}{\prod g^R} \exp\left(\frac{-(\sum E^L - \sum E^R)}{T^*}\right) \tag{3}$$

Where $g^{L(R)}$ and $E^{L(R)}$ are the statistical weight and the energy of a species at the left(right)-hand-side of the reaction, respectively, and T^* is the temperature governing the reaction, T_e for electron impact reactions and T for heavy species reactions.

Table 4. Electron impact reactions. Forward rate constants computed from the cross sections of the references.

No	Reaction	Ref	Note
eVs1	e + CO_2 ↔ e + CO_2v_a	[28]	A
eVs2	e + CO_2 ↔ e + CO_2v_b	[29]	A
eVs3	e + CO_2 ↔ e + CO_2v_c	[28]	A
eVa1	e + CO_2 ↔ e + CO_2v_1	[28]	B

Notes

A: For symmetric sublevels, e + CO_2v_n ↔ e + $CO_2v_{n,(a,b,c)}$. The cross sections are shifted according to the threshold energy of the reaction $E_{th} = E_{n,(a,b,c)} - E_n$.

B: The cross section is shifted and scaled for the excitation from an asymmetric level *n* to a higher asymmetric level *m*, e + CO_2v_n ↔ e + CO_2v_m. Fridman's approximation is used with scaling factors $\alpha = 0.5$ and $\beta = 0$ [10].

Table 4 lists the electron impact reactions included in the model. Through these reactions the kinetic energy of the electrons is transferred to the CO_2 molecule as vibrational energy. Due to the lack of experimental data the cross sections of the reactions shown in Table 4 are used to compute the cross sections of reactions involving higher vibrational levels. Reactions eVs1-3 correspond to the vibrational excitation of the first three symmetric levels and their cross sections are shifted to compute the cross sections of the analogous reactions forming symmetric sublevels, e + CO_2v_n ↔ e + $CO_2v_{n,(a,b,c)}$. This translation is done according to the threshold energy for the sublevel excitation $E_{th} = E_{n,(a,b,c)} - E_n$. The cross section for the vibrational excitation of the first asymmetric level, Reaction eVa1, is scaled and shifted to compute the cross section for the vibrational excitation from any asymmetric level *n* to a higher asymmetric level *m*, e + CO_2v_n ↔ e + CO_2v_m. Fridman's approximation[10] with scaling factors $\alpha = 0.5$ and $\beta = 0$ is used for the calculation of the cross sections. All cross sections are integrated with a Maxwellian EEDF for different electron temperatures to obtain the rate constants of the reactions as functions of the electron energy.

Table 5. Vibrational relaxation reactions. Rate constants in (m^3/s). VT: Vibrational-Translational (s: symmetric, a: asymmetric), VV': Intermode Vibrational-Vibrational, VV: Intramode Vibrational-Vibrational.

No	Reaction	Forward rate constant, $k_{k,\mathrm{f}}$	Ref	Note
VTs1	$CO_2v_a + CO_2 \leftrightarrow CO_2 + CO_2$	$7.14\times10^{-14}\exp\left(-177T^{-1/3}+451T^{-2/3}\right)$	30	A
VTs2	$CO_2v_b + CO_2 \leftrightarrow CO_2v_a + CO_2$	$1.94\times10^{-13}\exp\left(-177T^{-1/3}+451T^{-2/3}\right)$	30	A
VTs3	$CO_2v_c + CO_2 \leftrightarrow CO_2v_b + CO_2$	$2.90\times10^{-13}\exp\left(-177T^{-1/3}+451T^{-2/3}\right)$	30	A
VTa1	$CO_2v_1 + CO_2 \leftrightarrow CO_2v_a + CO_2$	$4.25\times10^{-7}\exp\left(-407T^{-1/3}+824T^{-2/3}\right)$	30	B
VTa2	$CO_2v_1 + CO_2 \leftrightarrow CO_2v_b + CO_2$	$8.57\times10^{-7}\exp\left(-404T^{-1/3}+1096T^{-2/3}\right)$	30	B
VTa3	$CO_2v_1 + CO_2 \leftrightarrow CO_2v_c + CO_2$	$1.43\times10^{-11}\exp\left(-252T^{-1/3}+685T^{-2/3}\right)$	30	B
VV'1	$CO_2v_1 + CO_2 \leftrightarrow CO_2v_a + CO_2v_b$	$2.13\times10^{-11}\exp\left(-242T^{-1/3}+633T^{-2/3}\right)$	30	C
VV1	$CO_2v_1 + CO_2v_1 \leftrightarrow CO_2 + CO_2v_2$	$1.8\times10^{-17}\exp\left(-24.7T^{-1/3}-65.7T^{-2/3}\right)$	13,31, 32	D

Notes
A: For symmetric sublevels, $CO_2v_{n,(a,b,c)} + CO_2 \leftrightarrow CO_2v_{n,(\ ,a,b)} + CO_2$.
B: Scale as $CO_2v_n + CO_2 \leftrightarrow CO_2v_{n-1,(a,b,c)} + CO_2$ for higher asymmetric levels.
C: Scales as $CO_2v_n + CO_2 \leftrightarrow CO_2v_{n-1,a} + CO_2v_b$ and $CO_2v_n + CO_2 \leftrightarrow CO_2v_{n-1,b} + CO_2v_a$ for higher asymmetric levels.
D: Scales as $CO_2v_n + CO_2v_m \leftrightarrow CO_2v_{n-1} + CO_2v_{m+1}$ for asymmetric levels *n* and *m*.

The vibrational relaxation reactions in the model include Vibrational-Translational relaxation (VT), Intramode Vibrational-Vibrational relaxation (VV) and Intermode Vibrational-Vibrational relaxation (VV'), see Table 5. In the VT relaxation process, energy is transferred between the vibrational and translational (heat) degrees of freedom. Reactions VTs1-3 correspond to VT relaxation of symmetric (sub)levels in a descending ladder fashion, i.e. $v_{(n,)c} \xrightarrow{\text{VTs3}} v_{(n,)b} \xrightarrow{\text{VTs2}} v_{(n,)a} \xrightarrow{\text{VTs1}} v_{(n)}$. The rate constants are assumed to be the same for the relaxation of symmetric sublevels as the asymmetric mode does not take part in the process.
Reactions VTa1-3 correspond to the VT relaxation of an asymmetric level *n* to a lower asymmetric level *n-1* with a symmetric sublevel *a*, *b* or *c*, i.e. $v_n \xrightarrow{\text{VTa1(2,3)}} v_{n-1,a(b,c)}$. The latter subsequently relaxes through reactions VTs1-3, losing its symmetric sublevels and becoming purely asymmetric again. Therefore, the combined effect of the VT reactions can be seen as an asymmetric VT relaxation process from level *n* to level *n-1*. Nevertheless, the addition of symmetric sublevels has an effect on the kinetics of this relaxation process.

In the VV' relaxation process, the energy is transferred between different vibrational modes, i.e. between the asymmetric and the symmetric modes in this case. Through this reaction, a fraction of the energy from the asymmetric mode is transferred to the symmetric modes of the collision partner. Thus, for a reacting asymmetric level *n*, the outcome is a lower asymmetric

level *n-1* with a symmetric sublevel *a* or *b* and the excitation of the ground state CO_2 to a symmetric level *b* or *a*, respectively, see Notes in Table 5. In the VV relaxation process the energy is transferred between levels of the same vibrational mode, i.e. the asymmetric mode in this model. This process is fast, nearly resonant, due to the small energy losses related to the anharmonicity of the molecule. Through this process, the vibrational energy predominantly flows toward higher levels due the lower energy requirement. The reverse process is not as efficient since the additional energy must be taken form the translational degree of freedom. The rate constants for the reactions VTa1-3, VV'1 and VV1 are computed as done by Kozak et al [12,13]. The complete reaction scheme for an asymmetric vibrational level *n* is illustrated in Figure 2.

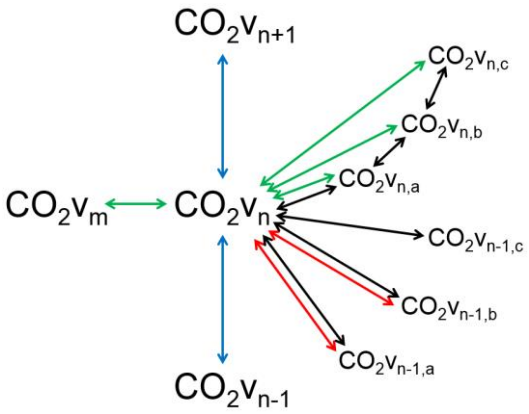

Fig. 2. Vibrational reactions scheme for a species CO_2V_n, showing eV reactions (green), VV relaxation (blue), VT relaxation (black) and VV' relaxation (red).

3. Results

The isothermal vibrational kinetics model was implemented in the Heavy Species Transport Module of the commercial software COMSOL Multiphysics (see Supporting Information for further details). This module can be configured to solve for equation 1 in a single 1D uniform element, having three parameters as inputs for the model: the electron mean energy $\bar{\varepsilon} = {}^{3}/_{2}\,T_e$, n_e and T. Pressure has no influence on the heavy species reactions as the number of reacting species is the same at either side of the reaction. The influence of the pressure on the electron impact reactions can be eliminated by choosing the electron density in a way that the ratio of electrons to neutral species, i.e. the ionization degree $\alpha = n_e\,/n_n$, remains unchanged for the same temperature T. The parameters were varied within the range of typical values for CO_2 dissociation experiments in non-thermal microwave plasmas, with $\bar{\varepsilon} = 0.75, 1.5, 2.25$ eV ($T_e = 0.5, 1, 1.5$ eV); $n_e = 10^{18}, 10^{19}, 10^{20}\ 1/\mathrm{m}^3$ and $T = 300 - 1500$ K, in steps of 200 K.

The temperature range is also restricted to these values due to the validity of the forward rate constant expressions[30]. The pressure was held constant at 100 torr for all calculations.

Figure 3 shows the steady state vibrational distribution functions (VDF) of the asymmetric mode for different set of reactions, at $T_e = 1$ eV (~11600 K), $T = 900$ K and $n_e = 10^{18}\ 1/\mathrm{m}^3$. The VDFs have been normalized to facilitate the comparison of results, thus, the shown densities correspond to the relative populations of the asymmetric vibrational levels $CO_2\nu_n$ with respect to the ground state CO_2. The Boltzmann distributions at the gas and electron temperatures are also shown for reference. These distributions are also obtained if vibrational relaxation (VV + VT + VV') and excitation processes (eV) are considered separately. Clearly, these processes are competing to bring the CO_2 species into thermal equilibrium with their corresponding driving temperatures, T or T_e. The VDFs that result from including both processes, relaxation and excitation, should therefore lie within these Boltzmann distributions. Nevertheless, as seen in Figure 3, the densities of high vibrational levels can exceed their corresponding densities of the Boltzmann distribution at T_e. When eV and VV reactions are considered together, the well-known Treanor distribution [33] is obtained. This distribution is the result of the vibrational excitation (determined by T_e), the vibrational energy exchange (determined by T) and the anharmonicity of the molecule. The combined effect is the preferential flow of vibrational energy to highly excited levels.

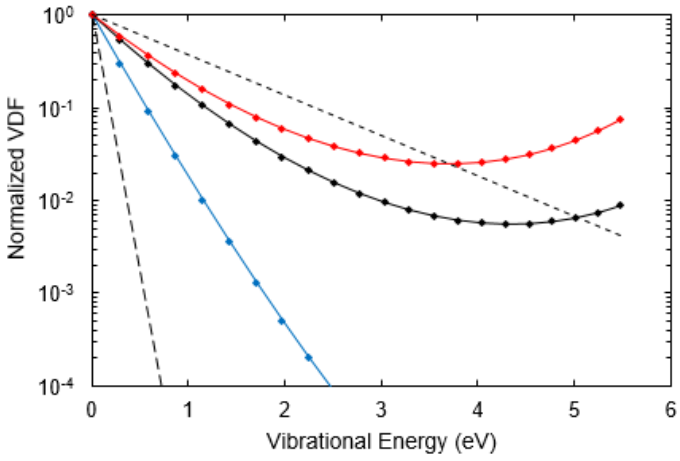

Fig. 3. Normalized steady state vibrational distribution function for different sets of reactions. Results with eV + VV in red (Treanor distribution), eV + VV + VT + VV' in black and eV + VV + VT + VV' without symmetric sublevels (Kozak) in blue. Boltzmann distributions at T (long dash) and at T_e (short dash) shown for reference. Calculations performed at $T_e = 1$ eV (~11600 K), $T = 900$ K and $n_e = 10^{18}\ 1/\mathrm{m}^3$.

Treanor-like VDFs can also be obtained when the processes for vibrational energy "loss", VT and VV', are included in the calculations. The VDF obtained for the complete vibrational kinetics model, shown in black in Figure 3, indicates that eV and VV dominate over VT and VV' at the mentioned conditions. Favorable conditions for the Treanor effect are high electron densities and low electron temperatures, to ensure high vibrational excitation rates, and low heavy species temperatures to maintain a low rate of vibrational energy loss. The rates of vibrational energy exchange (VV) are high even at low temperatures due to its nearly-resonant characteristic. Figure 3 also shows that a Treanor-like VDF was not obtained when an instant VT relaxation of the symmetric sublevels is assumed. This assumption neglects the sequential fashion of the VT relaxation of symmetric sublevels and therefore speeds up the VT relaxation of the asymmetric levels.

The vibrational excitation of the system is commonly indicated by the vibrational temperature, T_V, which should lie between the temperatures driving the competing processes, T_e and T. The vibrational temperature of the asymmetric mode, based on the first vibrational level, can be computed from $T_V = E_1/\ln(n_0/n_1)$. It is important to remark that this vibrational temperature refers to the departure from equilibrium of the first vibrational level and provides no information about the population of higher vibrational levels unless a defined VDF is assumed, e.g. Boltzmann or Treanor distribution.

Table 6 lists the steady state vibrational temperatures for the same sets of reactions of figure 3, with $T_e = 1$ eV, $n_e = 10^{18}\ 1/\mathrm{m}^3$ and $T = 300, 900$ and 1500 K. For the case of eV + VV reactions the vibrational temperature increases with the gas temperature. The reason for this behavior is that there is almost no vibrational energy lost to the translational mode, the gas temperature approaches the electron temperature and the rate of vibrational energy exchange increases, rising the Treanor distribution and partially straightening it as well. The effect of the symmetric sublevels in the complete vibrational kinetics model is also evident when comparing the vibrational temperatures obtained with and without these sublevels. At 300 K the effect of the symmetric sublevels is small, the vibrational temperatures are very close and the VDFs at the low energy region are similar. At 900 K the vibrational temperature obtained when considering the symmetric sublevels almost doubles the vibrational temperature obtained by assuming an instant relaxation of symmetric sublevels (see also figure 3). At 1500 K the VT relaxation rates further increase and difference between the vibrational temperatures decreases to 50%.

Table 6. Steady state vibrational temperatures in K for selected gas temperatures and sets of reactions. Calculations performed at $T_e = 1$ eV (~11600 K) and $n_e = 10^{18}\ 1/\mathrm{m}^3$.

	Gas Temperature (K)		
Reactions	**300**	**900**	**1500**
eV + VV	2762	6470	8274
eV + VV + VT + VV'	2967	5430	3045
eV + VV + VT + VV' (no sublevels)	3076	2802	2037

The variation in the vibrational temperatures of Table 6 can also be understood by analyzing the characteristics times of the kinetic processes in the plasma. These are computed from the rate constants of the reactions and the densities of colliding partners and provide insights into the timescales at which the different processes take place. The characteristic time for the electron impact vibrational excitation of the asymmetric mode is computed from the corresponding rate constant and the electron density, $\tau_{\mathrm{eVa}} = (k_{\mathrm{eVa1}}(T_e)n_e)^{-1}$. For electron temperatures between $0.5 - 1.5$ eV and an electron density of $10^{19}\ 1/\mathrm{m}^3$ this characteristic time has an order of magnitude of ~10^{-6} s. This value of the electron density corresponds to an ionization degree of $\sim 10^{-5}$ for a pressure of 100 torr and a gas temperature of 900 K. The characteristic times for vibrational relaxation are computed similarly and the results are presented in Table 7.

Table 7. Order of magnitude of characteristic relaxation times in (s), for a pressure of 100 torr and gas temperatures of 300 K and 1500 K.

Characteristic time	**300 K**	**1500 K**	**Note**
$\tau_{\mathrm{VTs}} = \left(k_{\mathrm{VTs}}(T)n_g(T)\right)^{-1}$	10^{-5}	$10^{-7} - 10^{-6}$	A
$\tau_{\mathrm{VTa}} = \left(k_{\mathrm{VTa}}(T)n_g(T)\right)^{-1}$	$10^{-4} - 10^{0}$	$10^{-7} - 10^{-5}$	B
$\tau_{\mathrm{VV'}} = \left(k_{\mathrm{VV'}}(T)n_{\mathrm{CO_2}}(T)\right)^{-1}$	10^{-5}	10^{-7}	C
$\tau_{\mathrm{VV}} = \left(k_{\mathrm{VV}}(T)n_{\mathrm{CO_2}}(T)\right)^{-1}$	10^{-9}	10^{-8}	D

Notes

A: VT relaxation of symmetric sublevels, $CO_2\nu_c \rightarrow CO_2\nu_b \rightarrow CO_2\nu_a \rightarrow CO_2$. Computed from rate constants of reactions VTs1-3 and gas density. The relaxation time is shorter for higher sublevels, $\tau_{\mathrm{VTs3}} \lesssim \tau_{\mathrm{VTs2}} \lesssim \tau_{\mathrm{VTs1}}$.

B: VT relaxation of asymmetric levels, $CO_2\nu_1 \rightarrow CO_2\nu_a$, $CO_2\nu_1 \rightarrow CO_2\nu_b$, $CO_2\nu_1 \rightarrow CO_2\nu_c$. Computed from rate constants of reactions VTa1-3 for the relaxation of the first asymmetric vibrational level. In general, for the studied temperature range, $\tau_{\mathrm{VTa3}} \approx \tau_{\mathrm{VTa2}} \ll \tau_{\mathrm{VTa1}}$.

C: VV' relaxation, $CO_2\nu_1 + CO_2 \rightarrow CO_2\nu_a + CO_2\nu_b$. Computed from the CO_2 density and the rate constant of reaction VV'1 for the relaxation of the first asymmetric vibrational level.

D: VV relaxation, $CO_2\nu_1 + CO_2 \rightarrow CO_2 + CO_2\nu_1$. Computed from the scaled rate constant of reaction VV1.

A quick comparison of the results in Table 7 indicates that the fastest process is VV relaxation and the slowest process is the VT relaxation of asymmetric levels (VTa). VV' relaxation takes place at timescales comparable to that of VT relaxation of symmetric sublevels (VTs). Indeed, symmetric sublevels are formed in the VV' relaxation and a lower asymmetric sublevel is attained only after VTs relaxation takes place. Since VTs relaxation takes place in a descending ladder fashion, the limiting step is the VT relaxation of the lowest symmetric sublevel *a*, which is the bottleneck of the process (see Note A in Table 7). Likewise, at high temperatures the VT relaxation of sublevel *a* also hinders the VTa relaxation, particularly the reactions whereby sublevels *b* or *c* are formed (see Note B in Table 7). Therefore, the relaxation of symmetric sublevels hinders the relaxation of asymmetric levels, resulting in Treanor-like VDFs (see Figure 3) and higher vibrational temperatures (see Table 6) when these are considered.

At low temperatures, the relation $\tau_{\mathrm{VV}} \ll \tau_{\mathrm{eVa}} < \tau_{\mathrm{VTs}} < \tau_{\mathrm{VTa}}$ holds. VV relaxation is ~3 orders of magnitude faster than electron impact vibrational excitation, implying that the latter limits the rate at which high vibrational levels are reached. In other words, significant excitation of high vibrational levels can only take place at timescales longer than ~10^{-6} s. Moreover, vibrational excitation and vibrational energy exchange processes are faster than vibrational energy loss processes, leading thus to an overpopulation of high vibrational levels (Treanor effect). At high temperatures, the relation is $\tau_{\mathrm{VV}} \ll \tau_{\mathrm{eVa}} \sim \tau_{\mathrm{VTs}} \sim \tau_{\mathrm{VTa}}$, with VV relaxation still ~2 orders of magnitude faster than electron impact vibrational excitation. VT relaxation takes place at shorter timescales, comparable to those of electron impact vibrational excitation, and therefore no significant vibrational excitation is achieved (see Table 6). For the conditions used in the calculation of the characteristic times, the vibrational kinetics model reaches the steady state at timescales of ~$10^{-4} - 10^{-3}$ s. However, the VDF is mostly developed at shorter timescales (~10^{-5} s) and slowly approaches its steady state form.

Table 6 shows that, for the complete kinetic model, the vibrational temperature increases as the gas temperature increases from 300 K to 900 K. At a gas temperature of 1500 K, the vibrational temperature decreases to approximately the same value obtained with a gas temperature of 300 K. This behavior is not observed in the non-thermal degree of the plasma, T_V/T, which is shown in Figure 4 for different values of the parameters T_e, n_e and T. This temperature ratio is an intrinsic comparison of VV and VT relaxation, which are competing processes in the vibrational energy transfer to higher levels. It is seen in figure 4 that T_V/T

decreases as the gas temperature increases for all combinations of the studied electron density and electron temperature values. Moreover, for high values of the electron density (top and middle graphs in Figure 4) the temperature ratio decreases in a very similar fashion. At higher temperatures it is expected that the curves approach the value of 1 and thus $T_V = T$, as clearly seen for the lowest electron density (bottom graph in Figure 4). In addition, for the lowest electron density and high electron temperatures, the decrease in the temperature ratio is not as smooth as seen in other curves of Figure 4. This is partially explained by the calculation method, in which the electron density and electron mean energy are fixed to specific values removing their inherent interdependency. The ionization rate coefficient is given by the ionization cross section and the EEDF. For a Maxwellian EEDF, the ionization rate coefficient increases with the electron temperature. The calculations were therefore performed considering all combinations of electron densities and electron temperatures, acknowledging that the calculation method decouples these variables.

Nonetheless, a rough estimate of the relation between the electron density and electron temperature can be obtained by solving the steady state of the electron impact ionization and dissociative recombination reactions for different values of the electron temperature. The total ionization cross section [28] of reaction e + CO_2 → 2e + CO_2^+ is used in the calculations. Likewise, the rate constant given by $2.0 \times 10^{-11} T_e^{-0.5} T_g^{-1}$ (m^3/s) [34] is used for the dissociative recombination reaction, e + CO_2^+ → CO + O. It is further assumed that CO and O instantaneously recombine to form CO_2 again. The results of these calculation are presented in Table 8.

Table 8. Steady state electron density for selected values of the electron temperature. Calculations performed at a pressure of 100 torr.

T_e (eV)	n_e $(1/m^3)$	α $(T = 300$ K)	α $(T = 1500$ K)
1.00	4.1×10^{17}	1.3×10^{-7}	6.4×10^{-7}
1.25	8.4×10^{18}	2.6×10^{-6}	1.3×10^{-5}
1.50	6.6×10^{19}	2.0×10^{-5}	1.0×10^{-4}
1.75	3.0×10^{20}	9.2×10^{-5}	4.6×10^{-4}
2.00	9.4×10^{20}	2.9×10^{-4}	1.5×10^{-3}

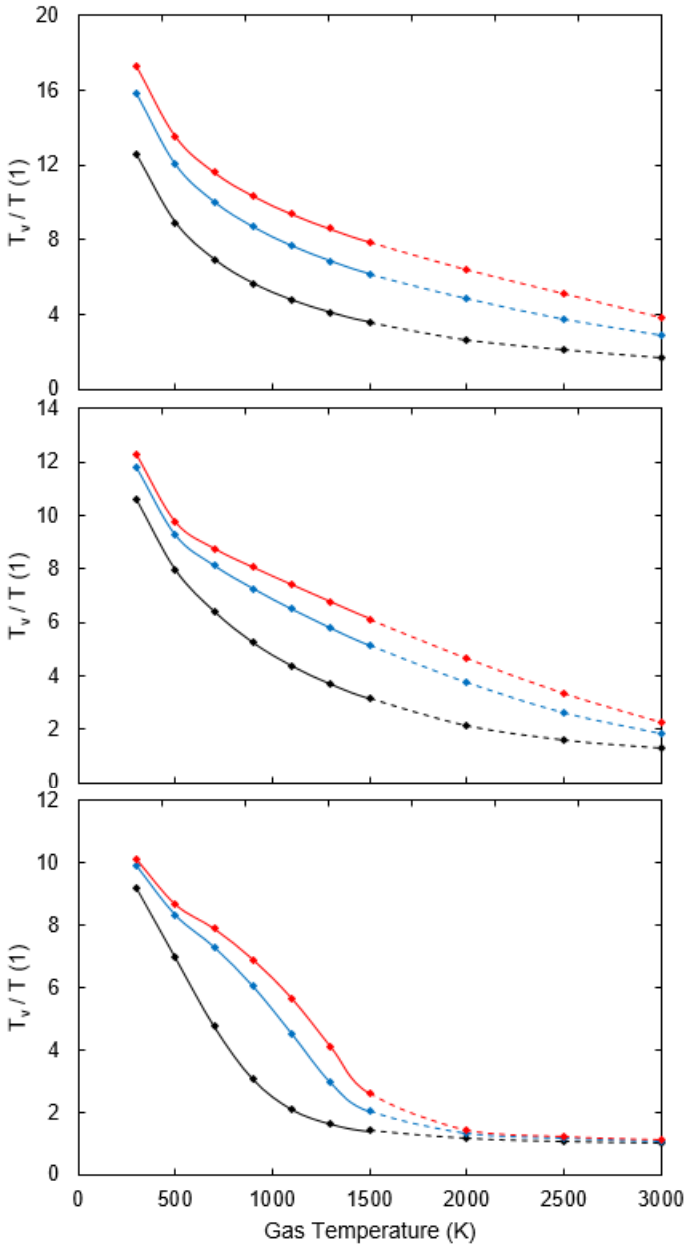

Fig. 4. Non-thermal degree, T_V/T, as function of the gas temperature. Computed with the complete vibrational kinetics model for electron densities of 10^{20} (top), 10^{19} (middle), 10^{18} $1/\mathrm{m}^3$ (bottom) and electron temperatures of 0.5 (black), 1.0 (blue), 1.5 eV (red). Solid lines cover the range of validity of rate constants in Table 5. Calculations inside this range of validity were performed in steps of 200 K, whereas steps of 500 K were used for temperatures higher than 1500 K.

Electron densities in orders of magnitude between 10^{17} and 10^{20} $1/m^3$ were obtained for electron temperatures between 1.00 and 2.00 eV, resulting in ionization degrees ranging from 10^{-7} to 10^{-3} in the gas temperature range of $300 - 1500$ K. The variation of the ionization degree with the gas temperature is due to expansion of the gas since the steady state electron density remains constant for the temperatures shown in Table 8. The non-thermal degrees

computed with these electron temperatures and densities are shown in Figure 5. As the gas temperature increases the non-thermal degree declines in a very similar way for all electron temperatures. However, at a very low ionization degree, the rates of vibrational excitation are also very low and for temperatures higher than ~1000 K the VT relaxation completely dominates and $T_V = T$ (see black dots in Figure 5).

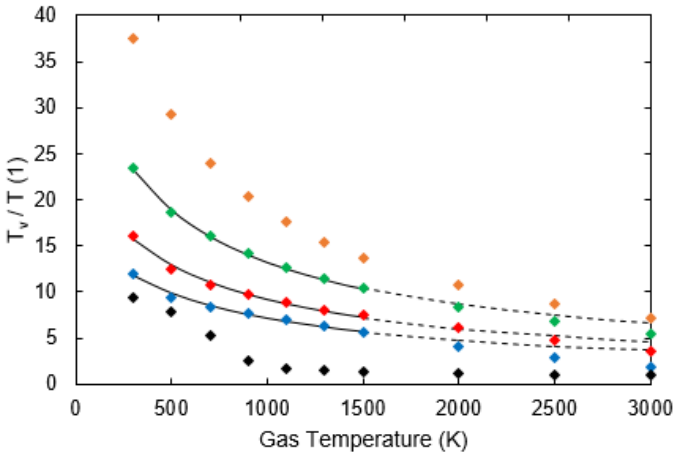

Fig. 5. Non-thermal degree, T_V/T, as function of the gas temperature. Computed with the complete vibrational kinetics model for the electron temperatures and corresponding electron densities given in Table 8: 1.00 (black), 1.25 (blue), 1.50 (red), 1.75 (green) and 2.00 eV (orange). Solid lines for the fitted functions within the range of validity of rate constants in Table 5, dashed lines for higher temperatures. Calculations inside this range of validity were performed in steps of 200 K, whereas steps of 500 K were used for temperatures higher than 1500 K.

Indeed, at high temperatures, the dots seem to approach the value of 1 at different gas temperatures. However, it is not possible to verify this in the model due to the temperature limitation in the validity of the rate constant expressions. At sufficiently high electron densities, the vibrational excitation and VV relaxation effectively compete against VT relaxation, and therefore the limit at which the non-thermal degree becomes 1 is when thermal equilibrium is reached and $T_e = T = T_V$.

The non-thermal degree data shown in Figure 5 can be fitted to the following expression with *A* and *B* being fitting parameters [23]

$$T_V/T = \frac{A}{T}\exp\left(\frac{B}{T^{1/3}}\right) \tag{4}$$

This expression incorporates the well-known Landau-Teller temperature dependence of VT relaxation, showing the strong influence of the gas temperature in the probability of energy transfer between the translation and vibrational degrees of freedom. This temperature dependence is also seen in the rate constant expressions of vibrational relaxation reactions in Table 5, although these also include a second order correction term.

Figure 5 shows the fitted curves for the electron temperatures and densities resulting in ionization degrees within the typical range of values, i.e. in the order of magnitude between 10^{-6} and 10^{-4} (see Table 8). The fittings were performed considering only the computed data in the gas temperature range of $300 - 1500$ K and have, in average, an Adjusted R-square higher than 0.99 and a Root Mean Square Error (RMSE) smaller than 0.22. These Goodness-of-Fit statistics are very good and validate equation 4 in the lower gas temperature range. At higher temperatures, outside the range of validity of rate constant expressions, the quality of the fitting decays. Nonetheless, the trends remain correct and the fitted curves approximately match the results of the vibrational kinetics model. It is to be noted that equation 4 can also describe the behavior of the steady state non-thermal degree when sublevels are not included.

Equation 4 has been previously used to approximate the evolution of the temperature ratio T_V/T with increasing gas temperatures [23,25] and dramatically reduce the vibrational kinetics of CO_2 in non-equilibrium microwave plasma. However, the origin of equation 4 was not addressed in detail in neither of those works as their purpose were to present a reduction methodology for vibrational kinetics and a two-step modelling approach for plasma reactors.

The reduction methodology is based on the wide difference in the timescales of the processes, especially at low gas temperatures. The characteristic times relation at low gas temperatures is $\tau_{\mathrm{VV}} \ll \tau_{\mathrm{eVa}} < \tau_{\mathrm{VTs}} < \tau_{\mathrm{VTa}} \ll \tau_{\mathrm{Diss}}$ (see Table 7 and subsequent discussion), where the characteristic time for CO_2 dissociation is the largest. The calculation of this characteristic time is performed for the first asymmetric vibrational level, assuming that its vibrational energy effectively reduces the energy barrier of the dissociation reaction[10]. Higher vibrational levels dissociate faster and the highest level, which lies in the dissociation limit, dissociates at timescales around ~10^{-10} s. Nevertheless, the formation of high vibrational levels is limited by the electron impact vibrational excitation and slowed down by the competing VT relaxation,

which implies that significant dissociation via vibrational excitation can only take place at timescales longer than ~10^{-6} s.

Therefore, in the reduction methodology the processes are divided into the very fast (immediate) VV relaxation and the slower competing processes that take place at longer, but similar timescales. VV relaxation is at least 10^2 times faster than slower processes in the gas temperature range of $300 - 1500$ K (10^3 times at low temperatures, see Table 7). Equation 4 is then used to update the T_V/T ratio at the longer timescales as VT relaxation proceeds and the gas temperature increases.

4. Conclusions

We have used a reaction kinetics model to study the vibrational kinetics of CO_2 plasma under the different conditions typically used in CO_2 dissociation experiments in non-thermal microwave plasmas. We showed that Treanor-like vibrational distribution functions can be obtained at low gas temperatures even if VT relaxation is included in the calculations. We also pointed out that symmetric sublevels can play an important role in defining the vibrational distribution function. In fact, at some conditions the vibrational temperature can almost double when VT relaxation of symmetric sublevels is accounted for in the model.

A timescale analysis of the collisional processes based on the first asymmetric vibrational level was performed to get insights into the behavior of the vibrational kinetics. It was found that, in general, VV relaxation is the fastest process and VT relaxation of asymmetric levels is the slowest process throughout the studied conditions. Moreover, it was found that the VT relaxation of symmetric sublevels limits the VV' relaxation process. Likewise, at high temperatures, the VT relaxation of asymmetric levels is hindered by the VT relaxation of symmetric sublevels, particularly the VT relaxation of asymmetric sublevels that proceed through the formation of symmetric sublevels *b* or *c*. Symmetric sublevels are formed in VV' and VT relaxation reactions. Their subsequent VT relaxation takes place in a descending ladder fashion, being the relaxation of the lowest level *a* the slowest step in the process. Therefore, it is concluded that the relaxation of symmetric sublevels slows down the relaxation of asymmetric levels and can lead to Treanor-like vibrational distribution functions and higher vibrational temperatures.

We also showed that, while T_V may increase with the gas temperature, the ratio T_V/T decreases with the gas temperature in the studied range of electron temperature and density values. It was also shown that above certain values of gas temperature, the VT relaxation is dominant; no vibrational excitation is attained and thus $T_V = T$. At sufficiently high electron densities, the limit at which the ratio T_V/T becomes 1 is when thermal equilibrium is reached and $T_e = T = T_V$.

Furthermore, we demonstrated that the behavior of the ratio T_V/T with increasing gas temperatures can be fitted to an expression that incorporates the Landau-Teller temperature dependence of VT relaxation. The fittings were evaluated by computing the Adjusted R-square and the Root Mean Square Error (RMSE), yielding both very good results in the gas temperature range of $300 - 1500$ K. Within this temperature range, the average Adjusted R-square is higher than 0.99 and the average Root Mean Square Error (RMSE) is smaller than 0.22. It is to be noted however, that at temperatures higher than 1500 K, the quality of the fittings decay, although the trends remain correct and the fitted curves approximately match the results of the vibrational kinetics model. This expression can therefore be used to approximately predict the ratio T_V/T at timescales longer than ~10^{-5} s, as VT relaxation proceeds and the gas temperature increases, particularly for ionization degrees greater than 10^{-6} and gas temperatures lower than ~1500 K.

Conflicts of interest

There are no conflicts to declare.

References

1 V. D. Rusanov, A. a. Fridman and G. V. Sholin, *Uspekhi Fiz. Nauk*, 1981, **134**, 185.

2 W. Bongers, H. Bouwmeester, B. Wolf, F. Peeters, S. Welzel, D. van den Bekerom, N. den Harder, A. Goede, M. Graswinckel, P. W. Groen, J. Kopecki, M. Leins, G. van Rooij, A. Schulz, M. Walker and R. van de Sanden, *Plasma Process. Polym.*, 2017, **14**, 1600126.

3 L. F. Spencer and A. D. Gallimore, *Plasma Sources Sci. Technol.*, 2013, **22**, 015019.

4 B. L. M. Klarenaar, M. Grofulović, A. S. Morillo-Candas, D. C. M. van den Bekerom, M. A. Damen, M. C. M. van de Sanden, O. Guaitella and R. Engeln, *Plasma Sources Sci. Technol.*, 2018, **27**, 045009.

5 T. Silva, N. Britun, T. Godfroid and R. Snyders, *Plasma Sources Sci. Technol.*, 2014, **23**, 025009.

6 T. Silva, N. Britun, T. Godfroid and R. Snyders, *Plasma Process. Polym.*, 2016, 1–4.

7 A. Vesel, M. Mozetic, A. Drenik and M. Balat-Pichelin, *Chem. Phys.*, 2011, **382**, 127–131.

8 N. den Harder, D. C. M. van den Bekerom, R. S. Al, M. F. Graswinckel, J. M. Palomares, F. J. J. Peeters, S. Ponduri, T. Minea, W. A. Bongers, M. C. M. van de Sanden and G. J. van Rooij, *Plasma Process. Polym.*, 2016, 1–24.

9 I. Belov, V. Vermeiren, S. Paulussen and A. Bogaerts, *J. CO2 Util.*, 2018, **24**, 386–397.

10 A. Fridman, *Plasma chemistry*, Cambridge University Press, 2008.

11 M. Capitelli, C. M. Ferreira, B. F. Gordiets and A. I. Osipov, *Plasma Kinetics in Atmospheric Gases*, Springer Berlin Heidelberg, Berlin, Heidelberg, 2000, vol. 31.

12 T. Kozák and A. Bogaerts, *Plasma Sources Sci. Technol.*, 2014, **23**, 045004.

13 T. Kozák and A. Bogaerts, *Plasma Sources Sci. Technol.*, 2015, **24**, 015024.

14 I. Armenise and E. Kustova, *J. Phys. Chem. A*, 2018, **122**, 8709–8721.

15 P. Diomede, M. C. M. van de Sanden and S. Longo, *J. Phys. Chem. C*, 2017, **121**, 19568–19576.

16 P. Diomede, M. C. M. van de Sanden and S. Longo, *J. Phys. Chem. A*, 2018, **122**, 7918–7923.

17 L. D. Pietanza, G. Colonna and M. Capitelli, *Plasma Sources Sci. Technol.*, 2017, **26**, 125007.

18 L. D. Pietanza, G. Colonna, G. D'Ammando and M. Capitelli, *Plasma Phys. Control. Fusion*, 2017, **59**, 014035.

19 M. Capitelli, G. Colonna, G. D'Ammando and L. D. Pietanza, *Plasma Sources Sci. Technol.*, 2017, **26**, 055009.

20 T. Silva, M. Grofulović, B. L. M. Klarenaar, A. S. Morillo-Candas, O. Guaitella, R. Engeln, C. D. Pintassilgo and V. Guerra, *Plasma Sources Sci. Technol.*, 2018, **27**, 015019.

21 E. V. Kustova and E. A. Nagnibeda, *Chem. Phys.*, 2006, **321**, 293–310.

22 E. V. Kustova and E. A. Nagnibeda, *Chem. Phys.*, 2012, **398**, 111–117.

23 J. F. de la Fuente, S. H. Moreno, A. I. Stankiewicz and G. D. Stefanidis, *React. Chem. Eng.*, 2016, **1**, 540–554.

24 A. Berthelot and A. Bogaerts, *Plasma Sources Sci. Technol.*, 2016, **25**, 045022.

25 S. H. Moreno, A. I. Stankiewicz and G. D. Stefanidis, *React. Chem. Eng.*, , DOI:10.1039/c9re00022d.

26 A. Berthelot and A. Bogaerts, *J. Phys. Chem. C*, 2017, **121**, 8236–8251.

27 I. Suzuki, *J. Mol. Spectrosc.*, 1968, **25**, 479–500.

28 M. Grofulović, L. L. Alves and V. Guerra, *J. Phys. D. Appl. Phys.*, 2016, **49**, 395207.

29 *Phelps database, www.lxcat.net, retrieved on January 10*, 2019.

30 J. A. Blauer and G. R. Nickerson, *A survey of vibrational relaxation rate data for processes important to CO2–N2–H2O infrared plume radiation*, Irvine, California, 1973.

31 T. G. Kreutz, J. a O'Neill and G. W. Flynn, *J. Phys. Chem.*, 1987, **91**, 5540–5543.

32 R. D. Sharma, *Phys. Rev.*, 1969, **177**, 102–107.

33 C. E. Treanor, *J. Chem. Phys.*, 1968, **48**, 1798.

34 R. E. Beverly, *Opt. Quantum Electron.*, 1982, **14**, 501–513.